**Annales
Geophysicae**

High-altitude and high-latitude O^+ and H^+ outflows: the effect of finite electromagnetic turbulence wavelength

I. A. Barghouthi[1,2], N. M. Doudin[1], A. A. Saleh[2], and V. Pierrard[3]

[1]Space Research Lab, Department of Physics, Al-Quds, University, P.O. Box 20002, Jerusalem, Palestine
[2]Department of Physics, Arab American University – Jenin , P.O. Box 240 Jenin, Palestine
[3]Belgian Institute for Space Aeronomy, 3 av. Circulaire 1180, Brussels, Belgium

Abstract. The energization of ions, due to interaction with electromagnetic turbulence (i.e. wave-particle interactions), has an important influence on H^+ and O^+ ions outflows in the polar region. The effects of altitude and velocity dependent wave-particle interaction on H^+ and O^+ ions outflows in the auroral region were investigated by using Monte Carlo method. The Monte Carlo simulation included the effects of altitude and velocity dependent wave-particle interaction, gravity, polarization electrostatic field, and divergence of auroral geomagnetic field within the simulation tube (1.2–10 earth radii, R_E). As the ions are heated due to wave-particle interactions (i.e. ion interactions with electromagnetic turbulence) and move to higher altitudes, the ion gyroradius ρ_i may become comparable to the electromagnetic turbulence wavelength $\lambda_\perp$ and consequently ($k_\perp \rho_i$) becomes larger than unity. This turns the heating rate to be negligible and the motion of the ions is described by using Liouville theorem. The main conclusions are as follows: (1) the formation of H^+ and O^+ conics at lower altitudes and for all values of $\lambda_\perp$; (2) O^+ toroids appear at 3.72 R_E, 2.76 R_E and 2 R_E, for $\lambda_\perp$=100, 10, and 1 km, respectively; however, H^+ toroids appear at 6.6 R_E, 4.4 R_E and 3 R_E, for $\lambda_\perp$=100, 10, and 1 km, respectively; and H^+ and O^+ ion toroids did not appear for the case $\lambda_\perp$ goes to infinity, i.e. when the effect of velocity dependent wave-particle interaction was not included; (3) As $\lambda_\perp$ decreases, H^+ and O^+ ion drift velocity decreases, H^+ and O^+ ion density increases, H^+ and O^+ ion perpendicular temperature and H^+ and O^+ ion parallel temperature decrease; (4) Finally, including the effect of finite electromagnetic turbulence wavelength, i.e. the effect of velocity dependent diffusion coefficient and consequently, the velocity dependent wave-particle interactions produce realistic H^+ and O^+ ion temperatures and H^+ and O^+ toroids, and this is, qualitatively, consistent with the observations of H^+ and O^+ ions in the auroral region at high altitudes.

Correspondence to: V. Pierrard
(viviane.pierrard@oma.be)

1 Introduction

Transversely accelerated ions at altitudes ranging from a few hundred kilometers to several Earth radii at auroral and polar cusp latitudes have been observed (Klumpar et al., 1984; Winningham and Burch, 1984; Arnoldy et al., 1992; Lundin et al., 1995; Eklund et al., 1997; Moore et al., 1999; Huddleston et al, 2000; Arvelius et al., 2005). The ion acceleration through wave-particle interaction with plasma turbulence at high latitudes of the Earth's magnetosphere has generally been accepted to explain the origin of the above observations. The effect of wave-particle interactions on ion outflows in the polar wind and auroral region is a subject of intense investigations, because the escape of the ionospheric ions to the magnetosphere is an important ionosphere/magnetosphere coupling mechanism. Therefore, several models have been developed to study the ion outflows and to explain the observations of the non-Maxwellian features of H^+ and O^+ ion velocity distributions at high latitudes. Chang and Coppi (1981) suggested a mechanism by which wave-particle interactions of ions with intense turbulence near lower hybrid frequency lead to ion conic formation observed by satellite, and consequently the intense lower-hybrid waves that are detected along the discrete auroral geomagnetic field lines could be the prime cause for the ion acceleration process. The plasma simulations of this mechanism (Retterer et al., 1986) predicted the simulations occurrence of counter streaming electrons that are commonly observed in conjunction with the ion conics in the supra-auroral region.

Retterer et al. (1987a) demonstrated that cyclotron resonance with observed electric field fluctuations is responsible for production of the oxygen-ion conic that are observed by the Dynamic Explorer 1 satellite in the central plasma-sheet

region of the Earth's magnetosphere. They described the ion velocity distribution by a quasi-linear diffusion equation which is solved by the Monte Carlo technique. Crew et al. (1990) presented a general theoretical treatment of energetic oxygen ion conics formation through cyclotron resonance with magnetospheric electromagnetic plasma turbulence; their theoretical predictions were found to be in excellent agreement with observations. Retterer et al. (1994) interpreted the data from the rocket campaigns MARIE and TOPAZ III, within regions of low-altitude transversely accelerated ions, to explain the acceleration of the ions. They found that the observed electric field amplitudes are sufficient to explain the observed ion energies in the MARIE event.

Brown et al. (1995) developed a generalized semi-kinetic model in order to study the transport of ionospheric plasma along auroral field lines. They obtained the formation of toroids and counterstreaming conics when a downward electric field is added to a case with wave heating. Wu et al. (2002) simulated ion outflow processes along auroral field lines with a dynamic fluid kinetic model which coupled a fluid ionospheric model to a semi-kinetic treatment for the topside through $3 R_E$ region. Large-scale extended parallel electric fields were incorporated in addition to the soft auroral electron precipitation and wave-driven ion-heating processes simulated in Wu et al. (1999). The ion velocity distribution evolves from bowl and suprathermal conic distributions at lower altitudes into mirrored conics and finally toroidal distributions at the top.

On the observational side, reports of toroidal ion distributions go back to Moore et al. (1985, 1986). The retarding ion mass spectrometer on DE 1 spacecraft revealed the occurrence of non-maxwellian suprathermal features in the auroral topside ionosphere distribution functions, and the appearance of an upgoing energetic tail having conical lobes as a common signature.

In a series of studies, Barakat and Barghouthi (1994a, b), Barghouthi and Barakat (1995), Barghouthi (1997), Barghouthi et al. (1998), Pierrard and Barghouthi (2006) and Barghouthi and Atout (2006) used Monte Carlo simulation to investigate the effect of wave-particle interaction on H^+ and O^+ outflows in the polar wind and auroral region. They reported that the effect of finite gyroradius is responsible for production of the H^+ and O^+ toroids at high altitudes equatorward of the cusp that are observed by TIDE and TIMAS ion instruments on board the polar spacecraft. They described the O^+ ion conics produced at $2 R_E$ on the auroral field lines by invoking the ion acceleration through wave-particle interaction (i.e. O^+ ions drift upward along geomagnetic field lines, they interact with electromagnetic turbulence and, consequently, get heated in the direction perpendicular to the geomagnetic field, the mirror force converts some of the ion energy gained in the perpendicular direction into parallel kinetic energy, these two effects combine to form an ion-conic distribution). Also, they found that the O^+

ions are preferentially heated owing to their mass and to the pressure cooker effect, the escape flux of O^+ was greatly enhanced while that of H^+ remained unchanged, both H^+ and O^+ ions are more energetic in auroral region than in polar wind at most altitudes, and the effect of body forces is more important in the polar wind and for O^+ ions than for auroral region and the H^+ ions.

In another series of papers, Bouhram et al. (2002, 2003a, b, 2004) studied the transverse heating and outflow of ions in the cusp/cleft region. Bouhram et al. (2002) studied the spatial properties of ionospheric ion outflows associated with perpendicular heating processes in the cusp using a conjunction study from two satellites and ground radar system. They presented an event of low-energy outflowing H^+ and O^+ populations observed by the Hyperboloid experiment aboard Interball Auroral Probe from 13 000 to 19 000 km altitude. These populations are observed over the dayside morning polar cap. They discussed the contribution of different energization mechanisms to the ion heating as a function of altitude. They found that since broadband extremely low-frequency turbulence is available to pre-heat the ions up to non-thermal energies, Lower Hybrid waves may provide additional energization up to keV energies for O^+ ions at high altitude.

Bouhram et al. (2003a), developed a two-dimensional, Monte Carlo, trajectory-based code for ion outflow from the dayside cusp/cleft, which is associated with transverse ion heating. They modeled the altitude dependence of ion cyclotron resonance heating from 1000 km to $3 R_E$ by a power law spectrum with an index α, and a parameter ω_0 that is proportional to the spectral density at a referenced frequency. They found that any triplet of (residence time of the ions when being energized, α, and ω_0) leads to a unique transport pattern feature of ion flows associated with a cusp/cleft ionospheric source. Bouhram et al. (2003b) used high-altitude (1.5–3 R_E) ion observation as constraints and the results of Bouhram et al. (2003a) are used to determine the altitude dependence of transverse ion heating during a significant number of the Interball-2 satellites. Bouhram et al. (2004) focused on the altitude dependence of oxygen ion conics in the dayside cusp/cleft region. They combined oxygen data from the Akebono, Interball-2, and Cluster satellites and followed the global development of the energetic (up to ∼10 keV) ion outflow over a continuous and broad altitude range up to about 5.5 R_E. They confirmed the results of Bouhram et al. (2003b), such as the fact that transverse ion heating in the cusp/cleft is height-integrated at radial distance below 4 R_E. The results inferred from Cluster observations put forward evidence of a saturation of both a transverse energization rate and ion gyroradii. Bouhram et al. (2004) interpreted these results in terms of finite perpendicular wavelength effects in the wave-particle interaction.

Barghouthi (1997) obtained an altitude dependent diffusion coefficient and Bouhram et al. (2004) derived velocity dependent diffusion coefficient. In this study, we will use a

combined (altitude part from Barghouthi, 1997, and the velocity part from Bouhram et al., 2004) form for the diffusion coefficient to investigate the H$^+$ and O$^+$ ion outflows in the equatorward of the cusp region. The paper is organized as follows: Theoretical formulations are provided in Sect. 2. In Sect. 3, we present the Monte Carlo model. The effects of altitude and velocity dependent wave-particle interactions on H$^+$ and O$^+$ outflows are presented and discussed in Sect. 4. The conclusions are presented in Sect. 5.

2 Theoretical formulations

In this paper, we study the steady state flow of a fully ionized plasma (H$^+$, O$^+$, and electrons) along the auroral geomagnetic field lines in the high-latitude topside ionosphere (i.e., the auroral region). The ions move under the effect of body forces (gravitational and polarization electrostatic fields) and mirror force due to the divergence of the auroral geomagnetic field lines. During their motion, the ions interact with the electromagnetic turbulence; the simulation region is a geomagnetic tube extending from the exobase at $1.2\,R_E$ to $10\,R_E$. The geomagnetic field was taken to be proportional to r^{-3} where r is the geocentric distance. In the absence of wave-particle interactions, the ion motion can be described by Liouville theorem (Barakat and Schunk, 1983), conservation of energy, conservation of the first adiabatic invariant (μ), and the ion velocity distribution function at the exobase. Invoking these conditions, we can calculate the ion velocity distribution at any point in the simulation region for a given potential energy profile ($\phi(r)$). The resulting relation can be solved simultaneously with the expression for ($\phi(r)$) and the quasi-neutrality condition:

$$\Phi(r) = kT_e \ln\left(\frac{n_e}{(n_e)_o}\right) + GM_e m\left(\frac{1}{r_0} - \frac{1}{r}\right) \quad (1)$$

$$n_e \cong n(\mathrm{O}^+) + n(\mathrm{H}^+) \quad (2)$$

where k is Boltzmann's constant, T_e is electron temperature, n_e and n_{e0} are the electron densities at r and r_0, respectively, G is the universal gravitational constant, M_E is the mass of the Earth, and m is the ion mass.

The effects of wave-particle interactions are represented by particle diffusion in the velocity space (Retterer et al., 1987a):

$$\left[\frac{\partial f}{\partial t}\right]_{\mathrm{WPI}} = \left(\frac{1}{v_\perp}\right)\frac{\partial}{\partial v_\perp}\left[D_\perp v_\perp \frac{\partial f}{\partial v_\perp}\right] \quad (3)$$

where ($D_\perp$) is the quasi-linear velocity diffusion rate perpendicular to geomagnetic field lines and is given by the following expression (Retterer et al., 1987b):

$$D_\perp = \frac{q^2}{m^2}\sum_{n=-\infty}^{\infty}\int\frac{d\omega}{2\pi}\int\frac{d^3K}{(2\pi)^3}\left[\frac{n\Omega}{\omega}\right]^2$$
$$A_n\pi\delta\left(\omega - n\Omega - k_\parallel v_\parallel\right) \quad (4)$$

with

$$A_n = \frac{1}{2}J_{n-1}^2|E_L|^2(k,\omega) + \left[\frac{v_\parallel J_n^2}{v_\perp}\right]^2|E_\parallel|^2(k,\omega)$$
$$+ \frac{1}{2}J_{n+1}^2|E_R|^2(k,\omega) \quad (5)$$

In these equations, q is the ion charge, m is the ion mass, Ω is the ion gyrofrequency, ω is the angular frequency of the electromagnetic turbulence, k is the wave vector, $J_n = J_n\left(\frac{k_\perp v_\perp}{\Omega}\right)$ is the standard Bessel function, and $|E_L|^2$ and $|E_R|^2$ are the spectral densities of the electric field in the two perpendicular polarizations. Retterer et al. (1987b) assumed $\left(k_\parallel v_\parallel \ll \Omega\right)$, $n=1$ and $\left(\frac{k_\perp v_\perp}{\Omega} \ll 1\right)$, and found that:

$$D_\perp = \frac{\eta q^2}{4m^2}|E_x(\omega = \Omega)|^2 \quad (6)$$

where $|E_L|^2(\omega) = \eta|E_x|^2(\omega)$, $|E_x|^2$ is the measured spectral density of the electromagnetic turbulence, and η is the proportion of the measured spectral density by plasma wave instrument (PWI) on board the DE-1 spacecraft that corresponds to the left hand polarized wave. This velocity diffusion rate, $D_\perp$, given in Eq. (6) is independent of velocity, and it depends on position (altitude) through the variation of the ion gyrofrequency, Ω, along the geomagnetic field lines. To improve the altitude dependence of $D_\perp$, Barghouthi (1997) and Barghouthi et al. (1998) processed the data collected by PWI on board the DE-1 spacecraft. They obtained the following expressions for $D_\perp$ in the region equatorward of the cusp.

$$D_\perp(r) = \begin{cases} 4.45 \times 10^7 (r/R_E)^{7.95}\,\mathrm{cm^2\,s^{-3}}, & \text{for H}^+, \\ \\ 6.94 \times 10^5 (r/R_E)^{13.3}\,\mathrm{cm^2\,s^{-3}}, & \text{for O}^+. \end{cases} \quad (7)$$

However, the adoption of this altitude dependent diffusion coefficient and similar ones such as that adopted by Crew et al. (1990), Barghouthi (1997), and Barghouthi et al. (1998) results in unrealistically high H$^+$ and O$^+$ ion temperatures at high altitudes. Also, it did not explained the non-Maxwellian features of ions at middle ($\sim 4\,R_E$) and high ($\sim 8\,R_E$) altitudes, such as H$^+$ and O$^+$ ion toroids and H$^+$ and O$^+$ ions temperatures. The description of these non-Maxwellian features requires a velocity dependent diffusion rate as suggested by Retterer et al. (1994).

Bouhram et al. (2004) obtained the velocity dependence of the diffusion coefficient, $D_\perp$. They found:

$$D_\perp \alpha J_0^2(k_{\perp 0}\rho_i) = J_0^2\left(\frac{k_{\perp 0}v_\perp}{\Omega_i}\right) = J_0^2\left(\frac{2\pi v_\perp}{\lambda_{\perp 0}\Omega_i}\right) \quad (8)$$

where $\rho_i = v_\perp/\Omega_i$ denotes the ion gyroradius, $k_\perp$ is the perpendicular component of the wave vector k, Ω_i is the ion gyrofrequency, and J_0 is the zeroth order of standard Bessel

function. Therefore, to model the ion perpendicular heating process, we specified a model for $D_\perp$ as a function of perpendicular velocity $v_\perp$ and position r/R_E along the auroral geomagnetic field line. For the velocity dependence, we chose the above form obtained by Bouhram et al. (2004), while for the altitude dependence we chose the form calculated by Barghouthi (1997). Altogether, the velocity and altitude dependent diffusion coefficient is written:

$$D_\perp(r, v_\perp) = \begin{cases} 4.45 \times 10^7 (r/R_E)^{7.95} J_0^2 \left(\frac{2\pi v_\perp}{\lambda_{\perp 0}\Omega_i}\right) \text{ cm}^2 \text{ s}^{-3}, \text{ for H}^+, \\ 6.94 \times 10^5 (r/R_E)^{13.3} J_0^2 \left(\frac{2\pi v_\perp}{\lambda_{\perp 0}\Omega_i}\right) \text{ cm}^2 \text{ s}^{-3}, \text{ for O}^+. \end{cases} \quad (9)$$

According to Eq. (9), in the infinite wavelength limit, e.g. $k_{\perp 0}\rho_i \ll 1$, $J_0 \sim 1$, we obtain the expression calculated by Barghouthi (1997) which does not depend on the ion velocity and, therefore, does not constrain the ion gyrating motion to the perpendicular scale size of the structures. However, for values of $k_{\perp 0}\rho_i \sim 2.4$, the term $J_0^2 (2\pi v_\perp/\lambda_{\perp 0}\Omega_i)$ tends to lower the heating rate (Bouhram et al., 2004), and for $k_{\perp 0}\rho_i \gg 2.4$, the effect of wave-particle interactions becomes negligible and the body and mirror forces control the motion of the ion.

3   Monte Carlo model

We will solve the kinetic Eq. (3) for the ion velocity distribution using a Monte Carlo model which was developed to investigate problems of this kind (Barghouthi, 1997). We considered the steady state flow of three components plasma composed of H⁺, O⁺, and electrons. The simulation region was a geomagnetic tube extending from $1.2 R_E$ to $10 R_E$. The ions were injected at $1.2 R_E$ with velocity consistent with a drifting Maxwellian distribution function. The ion motion was followed for a small time interval (Δt) as it moved under the influence of gravity, polarization electric field, and diverging geomagnetic field. The wave-particle interactions are taken into account by perturbing the ion velocity perpendicular to $\boldsymbol{B}$, ($v_\perp$), with a random increment ($\Delta v_\perp$) such that:

$$\left\langle (\Delta v_\perp)^2 \right\rangle = 4D_\perp(r, v_\perp)\Delta t \quad (10)$$

A large number of ions (H⁺ or O⁺) are followed (one at a time), where they are monitored as they cross a predetermined set of altitudes. The accumulated data at the monitoring altitudes are used to calculate the H⁺ and O⁺ ion velocity distributions and the H⁺ and O⁺ ions moments.

Since the data collected by the PWI instrument on board DE-1 spacecraft do not include information about $\lambda_\perp$, detailed information about $\boldsymbol{k}$-spectrum of the electromagnetic turbulence is unavailable. Owing to this, we considered a wide range of characteristic wavelengths for electromagnetic turbulence [$\lambda_\perp = \infty$, 100, 10, 1 km]. The boundary conditions selected for the auroral region are similar to those of

Barghouthi (1997). In practice, an iterative approach was used to find the electrostatic potential in a consistent manner. The model was run to solve the case of altitude dependent and velocity independent WPI as a starting point. The resulting electrostatic potential and consequently, the potential energy due to body force, Eq. (1), was then used in the model to find $n(\text{O}^+)$ and $n(\text{H}^+)$ with altitude and velocity dependent wave-particle interactions, which were substituted in Eqs. (2) and (1) in order to compute and improved value of $\phi(r)$. The new profile of $\phi(r)$ was then used to compute new density profile. The iteration process was continued until convergence was reached, which happened to occur in few (2–3) steps.

4   Results

The Monte Carlo model above is used to calculate the O⁺ and H⁺ ions velocity distributions f_i and the following lower order velocity moments:

$$n_i = \int f_i d^3 v_i \quad (11)$$

$$u_i = \frac{1}{n_i} \int v_{i\parallel} f_i d^3 v_i \quad (12)$$

$$T_{i\parallel} = \frac{m_i}{n_i k} \int \left(v_{i\parallel} - u_i\right)^2 f_i d^3 v_i \quad (13)$$

$$T_{i\perp} = \frac{m_i}{2n_i k} \int v_{i\perp}^2 f_i d^3 v_i \quad (14)$$

In the above equations, i denotes the type of ion (O⁺ or H⁺), n_i, u_i, $T_{i\parallel}$, and $T_{i\perp}$ are the ion density, drift velocity, parallel temperature, and perpendicular temperature, respectively.

Figure 1 shows the O⁺ velocity distribution $f(\text{O}^+)$ at different altitudes and for different values of electromagnetic turbulence wavelength $\lambda_\perp$. For the case of $\lambda_\perp = \infty$ (i.e. the velocity dependence of $D_\perp$ was not taken into consideration), the results are consistent with those of Barghouthi (1997). At $1.2 R_E$, $f(\text{O}^+)$ is consistent with the boundary conditions, and as the altitude increases, the distribution function develops conic features at $1.8 R_E$ and beyond. The formation of ion conics is due to altitude dependent wave-particle interaction, which heats the ions in the perpendicular direction, and to the mirror force, which converts some of the energy gained in the perpendicular direction to the parallel direction. At higher altitudes, the ion velocity distribution $f(\text{O}^+)$ saturates owing to dominant wave-particle interaction. Also, as mentioned in Sect. 2, for small infinite wavelength limit, $k_{\perp 0}\rho_i \ll 1$, $J_0 \sim 1$, i.e., the heating rate is independent of the ion velocity. For the case of $\lambda_\perp = 100$ km, $f(\text{O}^+)$ is similar to the case of $\lambda_\perp = \infty$ up to $\sim 2.76 R_E$. At altitude ($\sim 3.72 R_E$), the distribution function displays toroidal features. This toroidal shape can be explained if we remember that $D_\perp$ (Eq. 9) peaks near $v_\perp \cong 0$, and decreases
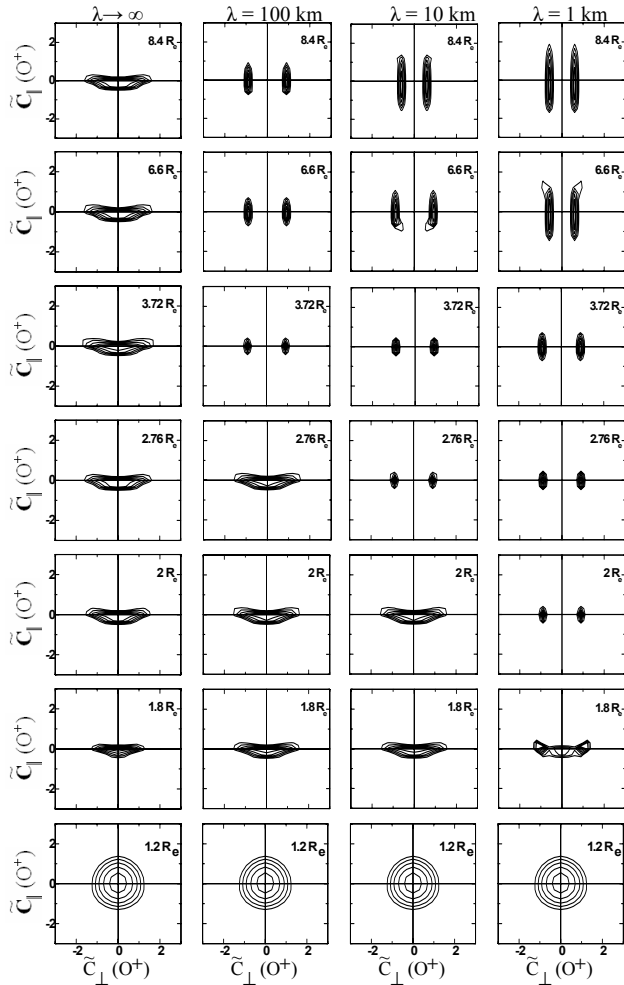
Fig. 1. O$^+$ ions velocity distribution functions at different geocentric distances (1.2, 2.0, 2.76, 3.0, 4.4, 6.6, and 7.2 R_E) for different electromagnetic turbulence wavelengths ($\lambda_\perp$), the wavelengths considered here are $\lambda_\perp \rightarrow \infty$, $\lambda_\perp$=100 km, $\lambda_\perp$=10 km, and $\lambda_\perp$=1 km. f (O$^+$) is represented by equal values contours in the normalized velocity ($\tilde{c}_\parallel$, $\tilde{c}_\perp$) plane, where $\tilde{c}=[v-u(\text{O}^+)]/[2kT(\text{O}^+)/m(\text{O}^+)]^{1/2}$. The contour levels decrease successively by a factor $e^{1/2}$ from the maximum.

very rapidly, as $J_0^2\left(\frac{k_\perp v_\perp}{\Omega_i}\right)$, for large values of $v_\perp$; therefore, the ions tend to move out of the region of large diffusion coefficient and accumulate in the region of relatively low $D_\perp$, forming the aforementioned toroidal distributions. At very high altitude ($\sim$6.6 R_E and above), the heating rate becomes negligible, and the effect of wave-particle interaction turns to be not significant. In the absence of wave-particle interactions, ions move under the effect of body forces (gravitational and polarization fields) and the mirror force due to the divergence of geomagnetic field. The ion motion can be described by Liouville theorem (Barakat and Schunk, 1983). At these high altitudes, f (O$^+$) develops temperature anisotropy, and
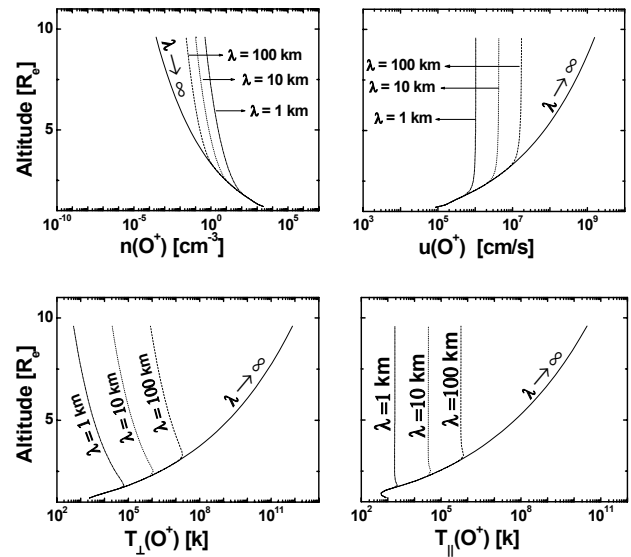

Fig. 2. Altitude profiles of the lower order O$^+$ moment for different electromagnetic turbulence wavelengths ($\lambda_\perp$). The wavelengths considered here are $\lambda_\perp \rightarrow \infty$ (solid), $\lambda_\perp$=100 km (dashed), $\lambda_\perp$=10 km (dotted), and $\lambda_\perp$=1 km (dashed dotted). The O$^+$ moments considered here are: density $n(\text{O}^+)$ (top left), drift velocity $u(\text{O}^+)$ (top right), perpendicular temperature T$_\perp$ (O$^+$)(bottom left), and parallel temperature T$_\parallel$ (O$^+$) (bottom right).

an asymmetry with an upward tail. The anisotropy is due to perpendicular adiabatic cooling, which occurs as O$^+$ ions drift upward into regions of lower magnetic field. The perpendicular temperature decreases in order to keep the conservation of the first adiabatic invariant μ. This explains the behavior of O$^+$ ions at 6.6 R_E and 8.4 R_E altitudes for the case of $\lambda_\perp$=100 km. As $\lambda_\perp$ decreases, the toroidal features appear at lower altitudes, at 2.76 R_E and 2 R_E for $\lambda_\perp$=10 km and 1 km, respectively. Also above these altitudes, the effect of wave-particle interactions becomes negligible and the motion of O$^+$ ions is described by Liouville theorem as mentioned above. Because, as $\lambda_\perp$ decreases, the argument of Bessel function, $\left(\frac{2\pi v_\perp}{\lambda_{\perp 0}\Omega_i}\right)$, increases, J_0 decreases and then the heating rate becomes negligible and the effect of wave-particle interaction turns to be negligible.

The effects of altitude and velocity dependent wave-particle interactions on the O$^+$ low-order velocity moments are presented in Fig. 2. Altitude profiles for ion density $n(\text{O}^+)$, drift velocity u(O$^+$), parallel temperature $T_\parallel(\text{O}^+)$, and perpendicular temperature $T_\perp(\text{O}^+)$ are given for $\lambda_\perp$=∞ (solid), $\lambda_\perp$=100 km (dashed), $\lambda_\perp$=10 km (dotted), and $\lambda_\perp$=1 km (dotted dashed). The top right panel of Fig. 2 shows the profiles of $u(\text{O}^+)$ for different values of $\lambda_\perp$. At low altitudes, the argument $k_{\perp 0}\rho_i$ is much lower than unity, and hence the profiles of $u(\text{O}^+)$ coincide for all values of $\lambda_\perp$, i.e., the effect of velocity dependent wave-particle interaction is negligible because $J_0 \sim 1$. For the
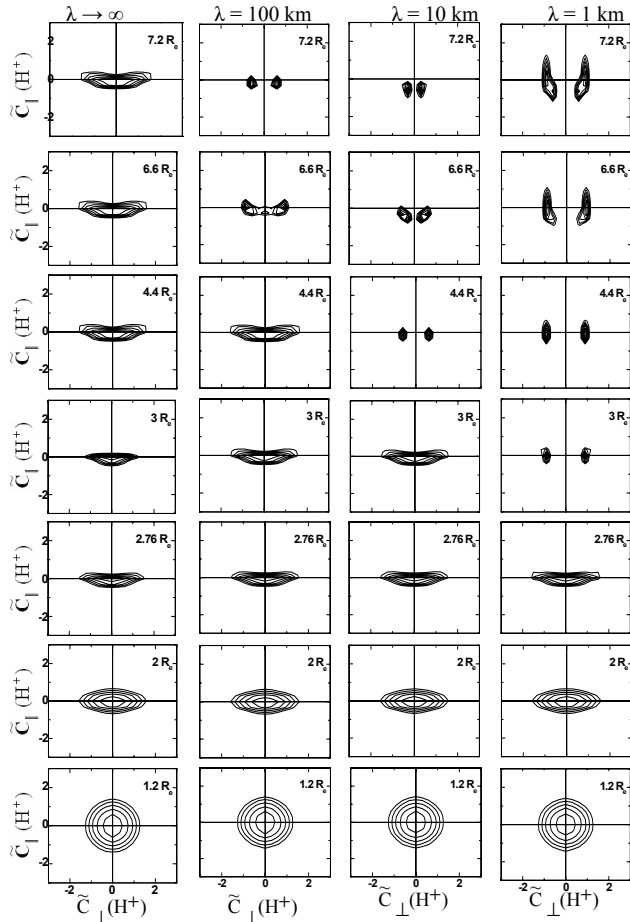
Fig. 3. H$^+$ ions velocity distribution functions at different geocentric altitudes (1.2, 2.0, 2.76, 3.0, 4.4, 6.6, and 7.2 R_E) for different electromagnetic turbulence wavelengths ($\lambda_\perp$), the wavelengths considered here are $\lambda_\perp \to \infty$, $\lambda_\perp = 100$ km, $\lambda_\perp = 10$ km, and $\lambda_\perp = 1$ km. $f\left(H^+\right)$ is represented by equal values contours in the normalized velocity ($\tilde{c}_\parallel$, $\tilde{c}_\perp$) plane, where $\tilde{c} = [v - u(H^+)] / [2kT\left(H^+\right)/m\left(H^+\right)]^{1/2}$. The contour levels decrease successively by a factor $e^{1/2}$ from the maximum.

case $\lambda_\perp = 100$ km, the heating (accelerating) rate and hence, $u(O^+)$ is reduced above the saturation level, 3 R_E, when compared to the case of ($\lambda_\perp = \infty$). This is an obvious result of the heating process because the heating rate decreases when $k_{\perp 0}\rho_i > 1$. As $\lambda_\perp$ decreases, $k_{\perp 0}\rho_i$ becomes greater than unity at lower altitudes and consequently the saturation level occurs at lower altitudes. Above the saturation level, the drift velocity is almost constant. This is due to the conservation of energy, because there is no heating and the motion is under the effect of body and mirror forces. Therefore, as $\lambda_\perp$ decreases, the drift velocity decreases because of the reduction of the heating rate, and O$^+$ density $n(O^+)$ (top left panel) increases to keep the escape flux constant (Barghouthi et al., 1998). The O$^+$ perpendicular temperature (bottom-left panel) monotonically increases for the case of $\lambda_\perp = \infty$,
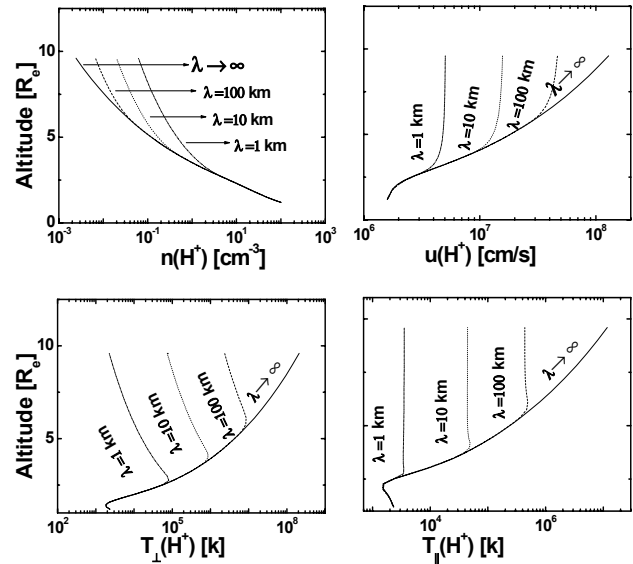

Fig. 4. Altitude profiles of the lower order H$^+$ moment for different electromagnetic turbulence wavelengths ($\lambda_\perp$). The wavelengths considered here are $\lambda_\perp \to \infty$ (solid), $\lambda_\perp = 100$ km (dashed), $\lambda_\perp = 10$ km (dotted), and $\lambda_\perp = 1$ km (dashed dotted). The H$^+$ moments considered here are: density $n(H^+)$ (top left), drift velocity $u(H^+)$ (top right), perpendicular temperature $T_\perp\left(H^+\right)$ (bottom left), and parallel temperature $T_\parallel\left(H^+\right)$ (bottom right).

and the model produces unrealistic temperatures at high altitudes ($\sim 10^{11}$ K). This is due to the heating in the perpendicular direction, which is occurred as a result of altitude dependent and velocity independent wave-particle interaction. However, including the effect of velocity dependent wave-particle interaction reduces $T_\perp(O^+)$, especially at high altitudes, to realistic temperatures. This reduction is expected because as $\lambda_\perp$ decreases, $k_{\perp 0}\rho_i$ becomes greater than unity and the heating rate turns to be negligible. The behavior of $T_\perp(O^+)$ above the saturation level is consistent with the features of the O$^+$ velocity distribution presented in Fig. 1. In the absence of wave-particle interaction, i.e. above the saturation level, the O$^+$ ions move under the effect of body and mirror forces and consequently, energy is transferred from perpendicular direction to the parallel direction in order to keep μ constant. The wave-particle interaction can influence the behavior of O$^+$ parallel temperature $T_\parallel(O^+)$ in two indirect ways (Barakat and Barghouthi, 1994a). First, the increased upward mirror force enhances the parallel adiabatic cooling. Second, the transfer of the energy from the perpendicular direction to the parallel direction tends to enhance $T_\parallel(O^+)$. The balance between these two effects determines the behavior of $T_\parallel(O^+)$.

Similarly, Fig. 3 presents the effect of altitude and velocity dependent wave-particle interaction on H$^+$ ion velocity distributions for different values of $\lambda_\perp$ and at different altitudes. For all values of $\lambda_\perp$, $f(H^+)$ is Maxwellian and

consistent with the boundary conditions at the exobase, and bi-Maxwellian at $2\,R_E$. This is due to perpendicular ion heating. The conic features appear at $2.76\,R_E$ and saturated for the case of $\lambda_\perp = \infty$. However, toroidal features appear at $6.6\,R_E$, $4.4\,R_E$, and $3\,R_E$, for $\lambda_\perp = 100$ km, 10 km, and 1 km, respectively. The behavior of $f(\mathrm{H}^+)$ at high altitudes for the case of $\lambda_\perp = 1$ km can be described in terms of Liouville theorem noted earlier. The difference between the behavior of O⁺ and H⁺ under the influence of altitude and velocity dependent wave-particle interactions is due to two factors. First, the large mass ratio ($m_{\mathrm{O}^+} = 16 m_{\mathrm{H}^+}$) and secondly, the preferential heating of O⁺ ions due to pressure cooker effect (Barakat and Barghouthi, 1994a). The heating rate is significant for $k_{\perp 0}\rho_i \geq 1$. Consequently, the saturation point occurs at higher altitudes for H⁺ than for O⁺.

Figure 4 shows the profiles of the lower order moment for H⁺ ions. The behavior of H⁺ ions below the saturation point (i.e., $k_{\perp 0}\rho_i < 1$) is the same for all values of $\lambda_\perp$ because $J_0 \sim 1$. Above the saturation point, H⁺ moments display trends similar to those of O⁺ moments as $\lambda_\perp$ decreases. For example, the drift velocity $u(\mathrm{H}^+)$ (top-right panel) decreases due to the reduction in the heating rate and consequently, the density $n(\mathrm{H}^+)$ (top left panel) increases to keep the net escape flux constant. Because of the significant reduction in the heating rate above the saturation point, H⁺ perpendicular temperature (bottom left panel) decreases in order to keep the first adiabatic invariant μ constant, and consequently $T_\parallel$ (O⁺) (bottom right panel) decreases, as $\lambda_\perp$ decreased.

In an on-going study, a comparison has been made between the above results and the results of other wave-particle interaction models with observations at high altitudes and high-latitudes. Qualitatively, the results of this model are comparable to the observations.

5 Conclusion

The effect of altitude and velocity dependent wave-particle interactions on O⁺ and H⁺ ions outflows was studied for conditions representative of the auroral region using a Monte Carlo simulation. In addition to the altitude and velocity dependent wave-particle interaction, we considered the body force (gravitational and polarization electrostatic) and the divergence of geomagnetic field lines. It was concluded that:

1. At low altitudes, the argument $k_{\perp 0}\rho_i$ was much less than unity and, consequently the results were independent of $\lambda_\perp$. Above a certain point called saturation point, the argument $k_{\perp 0}\rho_i$ became larger than unity and the heating rate turned to be very negligible.

2. Below the saturation point, the O⁺ and H⁺ ions velocity distributions displayed a conic features due to the effects of perpendicular heating and mirror force.

3. Above the saturation points, O⁺ and H⁺ velocity distribution displayed toroidal features, because the ions tend to diffuse out of the heating region in the velocity space.

4. The ion heating rate is dramatically decreased above the saturation point, because of the velocity dependence of $D_\perp$ on $J_0^2(k_{\perp 0}\rho_i)$.

5. As the electromagnetic turbulence wavelength $\lambda_\perp$ decreases, the ion heating rate decreased and the saturation point occurred at lower altitudes.

6. The saturation points of O⁺ ions occurred at lower altitudes than those of H⁺ ions.

In conclusion, the main effect of finite electromagnetic turbulence wavelength $\lambda_\perp$ on O⁺ and H⁺ outflows at high-altitude and high-latitude is to produce O⁺ and H⁺ toroids at the saturation point and to decrease the heating rate above the saturation point. Consequently, for large values of $\lambda_\perp$, the effect of wave-particle interactions turned to be not important, and then the ion outflow can be described by Liouville theorem.

References

Arnoldy, R. L., Lynch, K. A., Kintner, P. M., Vago, J. L., Chesney, S. W., Moore, T., and Pollock, C.: Burst of transverse ion acceleration at rocket altitudes, Geophys. Res. Lett., 19, 413–416, 1992.

Arvelius, S., Yamauchi, M., Nilsson, H., Lundin, R., Hobara, Y., Rème, H., Bavassano-Cattaneo, M. B., Paschmann, G., Korth, A., Kistler, L. M., and Parks, G. K.: Statistics of high-altitude and high-Latitude O⁺ ion outflows observed by Cluster/CIS, Ann. Geophys., 23, 1909–1916, 2005,
http://www.ann-geophys.net/23/1909/2005/.

Barakat, A. R. and Barghouthi, I. A.: The effects of wave-particle interactions on the polar wind O⁺, Geophys. Res. Lett., 21, 2279–2282, 1994a.

Barakat, A. R. and Barghouthi, I. A.: The effect of wave-particle interactions on the polar wind: Preliminary results, Planet. Space Sci., 42, 987–992, 1994b.

Barakat, A. R. and Schunk, R. W.: O⁺ ions in the polar wind, J. Geophys. Res., 88, 7887–7894, 1983.

Barghouthi, I. A.: Effects of wave particle interactions on H⁺ and O⁺ outflow at high latitude; A comparative study, J. Geophys. Res., 102, 22 065–22 075, 1997.

Barghouthi, I. A. and Atout, M. A.: Monte Carlo modeling of toroidal ion distributions and ion temperatures at high altitudes equatorward of the cusp: Effect of finite gyroradius, J. Geophys. Res., 111, A03202, doi:10.1029/2005JA011437, 2006.

Barghouthi, I. A. and Barakat, A. R.: Comparison between the wave-particle interaction in the polar wind and in the auroral region, Phys. Space Plasmas, 13, 445–450, 1995.

Barghouthi, I. A., Barakat, A. R., and Persoon, A. M.: The effects of altitude-dependent wave particle interactions on the polar wind plasma, Astrophys. Space Sci., 259, 117–140, 1998.

Bouhram, M., Dubouloz, N., Malingre, M., Jasperse, J. R., Pottelette, R., Senior, C., Delcourt, D., Carlson, C. W., Roth, I., Berthomier, M., and Sauvaud, J.-A.: Ion outflow and associated perpendicular heating in the cusp observed by Interball Auroral Probe and Fast Auroral Snapshot, J. Geophys. Res., 107(A2), 1023, doi:10.1029/2001JA000091, 2002.

Bouhram, M., Klecker, B., Miyake, W., Reme, H., Sauvaud, J.–A., Malingre, M., Kistler, L., and Blagau, A.: On the altitude dependence of transversely heated O^+ distributions in the cusp/cleft, Ann. Geophys., 22, 1–12, 2004,
http://www.ann-geophys.net/22/1/2004/.

Bouhram, M., Malingre, M., Jasperse, J. R., and Dubouloz, N.: Modeling transverse heating and outflow of ionospheric ions from the dayside cusp/clef: 1 A parametric study, Ann. Geophys. 21, 1753–1771, 2003a.

Bouhram, M., Malingre, M., Jasperse, J. R., Dubouloz, N., and Sauvaud, J.-A.: Modeling transverse heating and outflow of ionospheric ions from the dayside cusp/clef: 2 Applications, Ann. Geophys. 21, 1773–1791, 2003b.

Brown, D. G., Horwitz, J. L., and Wilson, G. R.: Synergistic effects of hot plasma-driven potentials and wave-driven ion heating on auroral ionospheric plasma transport, J. Geophys. Res., 100(A9), 17 499–17 514, 1995.

Chang, T. and Coppi, B.: Lower hybrid acceleration and ion evolution in the supraroral region, Geophys. Res. Lett., 8, 1253–1256, 1981.

Crew, G. B., Chang, T., Retterer, J. M., Peterson, W. K., Gurnett, D. A., and Huff, R. L.: Ion cyclotron resonance heated conics: Theory and observations, J. Geophys. Res., 95, 3959–3985, 1990.

Eklund, U., Lundin, R., and Sandahl, I.: Measurements of O^+ in the high latitude magnetosheath, Phys. Chem. Earth., 22, 639–644, 1997.

Huddleston, M. M., Pollock, C. J., Wuest, M. P., Pichett, J. S., Moore, T. E., and Peterson, W. K.: Toroidal ion distributions observed at high altitudes equatorward of the cusp, Geophys. Res. Lett., 27(4), 469–472, 2000.

Klumpar, D. M., Peterson, W. K., and Shelley, E. G.: Direct evidence for two-stage (bimodal) acceleration ionospheric ions, J. Geophys. Res., 89, 10 779–10 787, 1984.

Lundin, R., Woch, J., Yamauchi, M., and Marklund, G.: Boundary Layer polarization and voltage in the 14 MLT regions, J. Geophys. Res., 100, 7587–7597, 1995.

Moore, T. E., Chappel, C. R., Lockwood, M., and Waite Jr., J. H.: Suprathermal ion signatures of auroral acceleration processes, J. Geophys. Res., 90, 1611–1618, 1995.

Moore, T. E., Lundin, R., Alcayde, D., André, M., Ganguli, S. B., Temerin, M., and Yau, A.: Source processes in the High-Latitude ionosphere, Space Sci. Rev., 88, 7, 1999.

Moore, T. E., Waite Jr., J. H., Lockwood, M., and Chappell, C. R.: Observations of coherent transverse ion acceleration, in: Ion Acceleration in the Magnetosphere and Ionosphere, Geophys. Monogr. Ser., vol. 38, edited by: Chang, T., p. 50–55, AGU, Washington D.C., 1986.

Pierrard, V. and Barghouthi, I. A.: Effect of wave-particle interactions on double-hump H^+ velocity distribution in the polar wind, Astrophys. Space Sci., 302, 35–41, doi:10.1007/s/s10509-005-9002-y, 2006.

Retterer, J. M., Chang, T., and Jasperse, J. R.: Transversely accelerated ions in the topside ionosphere, J. Geophys. Res., 99, 13 189–13 201, 1994.

Retterer, J. M., Chang, T., Crew, G. B., Jasperse, J. R., and Winningham, J. D.: Monte Carlo modeling of ionospheric oxygen acceleration by cyclotron resonance with broad-band electromagnetic turbulence, Phys. Rev. Lett., 59, 148–151, 1987a.

Retterer, J. M., Chang, T., Crew, G. B., Jasperse, J. R., and Winningham, J. D.: Monte Carlo modeling of Oxygen ion conic acceleration by cyclotron resonance with broadband electromagnetic turbulence, Phys. Space Plasmas, 6, 97–111, 1987b.

Retterer, J. M., Chang, T., and Jasperse, J. R.: Ion acceleration by lower hybrid waves in the supraroral region, J. Geophys. Res., 91, 1609–1618, 1986.

Winningham, J. D. and Burch, J.: Observations of large-scale ion conic generation with DE-1, Phys. Space Plasmas, 5, 137–158, 1984.

Wu, X.-Y., Horwitz, J. L., Estep, G. M., Su, Y.-J., Brown, D. G., Richards, P. G., and Wilson, G. R.: Dynamic fluid-kinetic (DyFK) modeling of auroral plasma outflow driven by soft electron precipitation and transverse ion heating, J. Geophys. Res., 104(A8), 17 263–17 276, 1999.

Wu, X.-Y., Horwitz, J. L., and Tu, J.-N.: Dynamic fluid kinetic (DyFK) simulation of auroral ion transport: Synergistic effects of parallel potentials, transverse ion heating, and soft electron precipitation, J. Geophys. Res., 107(A1)0, 1283, doi:10.1029/2000JA000190, 2002.